The University of Tehran Press

Pollution

Print ISSN: 2383-451X
Online ISSN: 2383-4501

https://jpoll.ut.ac.ir/

Comparison of GO/CdNPs and GO/CuNPs Nanocomposites for CO Gas Sensing at 200 °C

Ibrahim Hammadi Frhan✉

Ministry of Education, Directorate of Anbar Education, Karma Education Department, Karma Preparatory School for Boys, Anbar, Iraq.

Article Info

Article type:
Research Article

Article history:
Received: 5 February 2026
Revised: 20 March 2026
Accepted: 5 April 2026

Keywords:
Nano
Sensor
Graphene Oxide
Nanoparticle
Sensitivity
Plasma

ABSTRACT

The thickness of the nanocomposite films used is 22 and their area is 50 micrometers. The concentration of CO gas used is 20 ppm, proportional to the weight of the nanosensor (0.02%). The plasma technique was used to prepare the (CdNPs) and (CuNPs) nano-metals. The response time for CdNPs was 13.5s at 25°C, 22.5s at 100°C, and 19.8s at 200°C. For CuNPs, the response time was 24.7s at 25°C, 24.7s at 100°C, and 23.4s at 200°C. The FAAS method was used to identify these nanometals and determine their concentrations. Additionally, FTIR, UV-Vs, FESEM, EDX, and XRD methods were used to diagnose it. Additionally, a nanocomposite of oxide and nanometals with a mixing ratio of 10:1:1 is created by preparing graphene oxide using the Hummer process. The (GO/CdNPs) nanocomposite was tested for gaseous sensitivity to CO gas in comparison to the (GO/CuNPs) nanocomposite, and the results showed good sensitivity to the gas.

Cite this article: Hammadi Frhan, I. (2026). Comparison of GO/CdNPs and GO/CuNPs Nanocomposites for CO Gas Sensing at 200 °C. *Pollution*, 12(2), 732-750.
https://doi.org/10.22059/poll.2026.413790.3326

 Publisher: The University of Tehran Press.
DOI: https://doi.org/10.22059/poll.2026.413790.3326

INTRODUCTION

Environmental pollution are pyrolysis and burning of materials can produce several harmful combustion products that cause irritation, incapacitation, systemic toxicity, asphyxiation, and even fatal exposures after brief encounters. Common harmful substances in fire effluent include complex molecules like polycyclic aromatic hydrocarbons, nitrogen oxides (NOx), asphyxiant gases like carbon monoxide (CO) and hydrogen cyanide (HCN), (and irritants such as acrolein and phosgene. These issues affect many people and are primarily caused by industrial activities (Rashid et al., 2024). Nowadays, the advancement of low cost, compact and fast sensors have become an area of great potential. There are various toxic gases (CO, NO2, SO2, CO2 etc) in the environment which are hazardous to living things. For instance, the incomplete combustion of fossil fuels including natural gas are responsible for emission of CO gas (Kumar et al., 2022). Powders and materials optimized at the nanoscale (1–100 nm) are known as nanomaterials. The ideas of classical and quantum physics are no longer applicable at the nanoscale, and a wide range of unanticipated features are conceivable. Materials having unique or greatly improved characteristics can be used in new applications (Lines et al., 2008). Applications,

*Corresponding Author Email: *ibrahim.hum69@gmail.com*

manufacturing, and processing of materials smaller than 1000 nm a nanometer is one billionth of a meter are the focus of nanotechnology. Researchers from chemistry, physics, biology, and engineering collaborate in the multidisciplinary discipline of nanoscience, which sparks intense interest across numerous sectors (Rashid, 2024). Numerous changes in physical attributes can result from the transition from microparticles to nanoparticles. The size of the particle entering the domain where quantum effects predominate and the rise in the surface area to volume ratio are two of the main causes of this (Ruiz et al., 2024). As a particle gets smaller, the surface-area-to-volume ratio gradually increases, which causes the behavior of atoms on a particle's surface to become more dominant than that of atoms inside the particle (López-Hernández, 2021). This influences the particle's characteristics both on its own and when it interacts with other substances (Vargas et al.,2021) In order to improve the performance of technologies like fuel cells and batteries, high surface area is essential for catalysis and structures like electrodes (Pan et al., 2024).

The term "nanotechnology" appears in the media almost daily. Nanotechnology enables the creation of materials with improved electrical, magnetic, optical, and chemical capabilities using building blocks the size of atom clusters (Geng et al., 2024). Beyond the intrinsic "economy of geometry" of downsizing, the improved characteristics offer far greater potential. These characteristics include toughness, photoluminescence, hydrophobicity, and transparency (Lines et al.,2008). As well as bioavailability, chemical sensitivity, and hardness (Naseem et al.,2025). Products made from these materials have special qualities and a variety of high-value commercial uses in quickly growing markets (Tofail et al.,2018). Small particle size, narrow size distribution, low levels of agglomeration, and great dispersibility are the essential attributes required by nanoparticles to capture high-value markets (Gao et al.,2025). The idea that structures could be created is the source of the intense interest in nanotechnology (Malik et al.,2023). and constructed with better mechanical, electrical, chemical, or optical qualities than the materials we now use (Salim et al.,2024). Products are typically made by etching away at materials to reduce their size (Oehrlein et al.,2024). On the other hand, nanotechnology starts with something at the molecular level and builds upon it one atom or molecule at a time (Oehrlein et al.,2024). There are two primary methods for producing nanoparticles (Altammar.,2023). The conventional approach of creating small particles has been "top-down," which refers to the reduction through attrition and different conventional methods of combustion (Chen et al.,2022). The use of "bottom up" production processes has grown during the last many years (Orangi et al.,2024). Research on smart, self-assembling materials with a variety of applications is producing performance potential never seen before (Chen et al.,2025).

Materials developers are interested in the special qualities of nanomaterials and nanoscale structures (Khan et al.,2025). Surface coatings, fillers in plastics, and UV protectants in cosmetics are just a few examples of how these materials are already being employed to slightly alter product performance (Coiai et al.,2021). A.however, the technology is more promising for the future and is anticipated to bring about more disruptive changes to markets and products (Lowry et al.,2025). Medical, plastics, energy, electronics, and aerospace are just a few of the industries where nanotechnology is making inroads. Despite being about one-sixth the weight of steel, carbon nanotubes have been shown to be 100 times stronger. They can be constructed into semiconductor-like structures or structures as electrically conductive as copper (Gao et al.,2025). The variety of nanomaterial is incredibly large therefore a selection follows but is by no means exhaustive (Ding et al.,2025). Hundreds of laboratories worldwide are developing new uses for nanomaterials. Some will discover practical uses that will fundamentally alter how we live in the coming years (Malik et al.,2023). In every area of technology, including automotive, aircraft, construction, electronics, medical, sensors, and computing, materials nanocomposites are essential to improving people's quality of life. As nanoscience has progressed, nanocomposites have become highly valuable materials for a range

of uses (Omanović-Mikličanin et al.,2020). Physics, chemistry, biology, materials science, and engineering are all included in the multidisciplinary field of nanocomposites. Novel science, and especially novel materials, with unanticipated technological potential like the fabrication of macroscopic manufactured materials through nanoscale structures, are produced by the expertise of scientists from diverse backgrounds. High mechanical, electrical, and thermal properties have been the goal of the design of several nanocomposites. An overview of the type, synthesis, characterization, characteristics, modeling, and applications of nanocomposites in many fields is provided in this work (Mirkin et al., 2025).

A promising development in this field, nanosensors defined as sensors that use nanomaterials to detect and measure compounds at the nanoscale offer the potential to transform aspirin detection and enhance patient outcomes in stroke therapy and other areas (Koohkansaadi et al., 2025).

MATERIALS & METHODS

Graphite was transformed into nano graphene oxide using the Hammers method. $KMnO_4$, 98% pure $H2SO_4$, and 98% pure $NaNO_3$ are the components utilized. by extracting nanometals from their chloride salts utilizing our specifically engineered plasma system. The method makes use of 5600 V of power and argon gas.

prepare graphene oxide

The Hummers technique was used to convert graphite into graphene oxide. An ice bath is used to chill a 1000 mL beaker filled with 96 mL of pure sulfuric acid (H_2SO_4). The reaction flask is filled with two grams of graphite, one gram of sodium nitrate ($NaNO_3$), and six grams of potassium permanganate ($KMnO_4$). (Liu et al., 2021). Since potassium permanganate raises the temperature, it should be added gradually. Keeping the temperature of the reaction below 10°C is crucial. After two hours of constant stirring, the mixture's color will change from black to green (Fig. 1-A).

The liquid is taken out of the ice bath and put on a hotplate with constant stirring for 36 hours at a temperature of 30 to 40°C. The color changes from green to a brownish yellow, as shown in (Fig. 1-B). The reaction mixture is then again immersed in an ice bath to keep the temperature from rising.

After that, gradually add the water while continuously stirring until the mixture reaches 500

Fig. 1: A. Representing the *first reaction step*, and the color turning green.

Fig. 1: B. showing the hue changing to brown after 36 hours and the second reaction step.

Fig. 1: C. Representing the *addition of H_2O and H_2O_2*

Fig. 1: D representing the *GO precipitate*.

ml. gradually add 5 mL of 30% hydrogen peroxide (H_2O_2) to the mixture and stir constantly for two hours. As shown in Figure 1-C, we see that the hue changes from light brown to dark brown or reddish brown.

First, centrifugation at 6000 R/S for 15 minutes is used to separate the top layer from

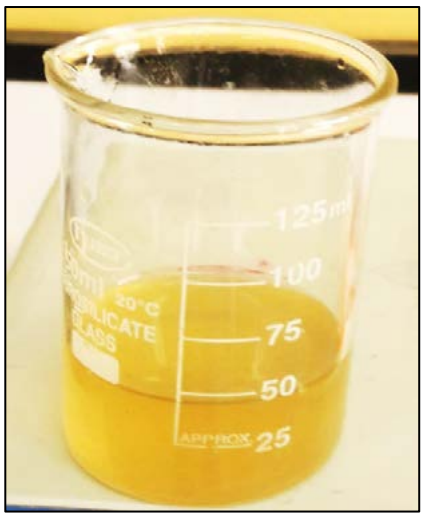

Fig. 2: demonstrates the color of the filtrate used to prepare graphene oxide.

the precipitate after the combination has been left for a full day (Fig. 1-D).The precipitate's brownish-black color is depicted in Fig. 1-E, whereas the filtrate's yellowish-orange color is shown in Fig. 2. Following the separation procedure, the precipitate, or graphene oxide, is washed three times with a 10% hydrochloric acid (HCl) solution.

The graphene oxide precipitate is repeatedly cleaned with deionized water until it reaches a stable pH function. After each washing stage, the components are separated using a centrifuge. The precipitate is dried for 24 hours at 60°C in a drying oven to eliminate the water. Next, wash with ethanol to remove any leftover contaminants. The precipitate is fully processed to produce a powder. To diagnose graphene oxide, a sample is subjected to FTIR analysis. The preparation process is repeated several times till the desired weight is reached.

Nanometal preparation with plasma technique

Recently, the plasma approach has been employed to extract nanometals from their chloride salts (Fanelli et al., 2014). A voltage of 5600 volts is utilized. When the pressure leaving the gas cylinder is kept at 10 bar, the ideal flow rate for argon gas is 2 cm^3/s. Both copper ($CuCl_2$) and cadmium ($CdCl_2$) chlorides are made. Make 1000 ppm concentrations of each metal salt in a 500 ml volumetric flask. A 75 ml beaker is filled with 40 ml of the volumetric flask containing the metal salts. The prepared salt solution is put 1.5 cm away from the solution's surface in a beaker that holds the cell's negative electrode. The positive electrode of the cell is connected to a 2 mm-diameter jet needle that allows argon gas to flow through it. The capillary tube is also one centimeter away from the surface of the fluid. Plasma is continually applied to the solution when the voltaic and gas apparatus is opened. The transition, which takes place over a few minutes, is indicated by the color shift of the solution. This change implies the formation of metal nanoparticles. This process is repeated several times until the prepared solution in the volumetric flask runs out. The temperature of the solution never rises above 40 °C when the plasma is present. Fig. (3) illustrates how cadmium and copper are transformed into nano cadmium and nano copper. When a colorless solution of cadmium chloride turns yellow, it has transformed into nanocadmium. In a similar vein, the transformation of blue copper chloride into nanocopper is shown by its color changing to green. A centrifuge set to 12,000 R/m is used to gather and separate these amounts of each element. After removing the precipitate, the appropriate amount of water (3 ml) is combined with it. Following the acquisition of the necessary amounts of metallic nanoparticles, samples are extracted from them for UV, XRD, FESE, and EDX analysis.

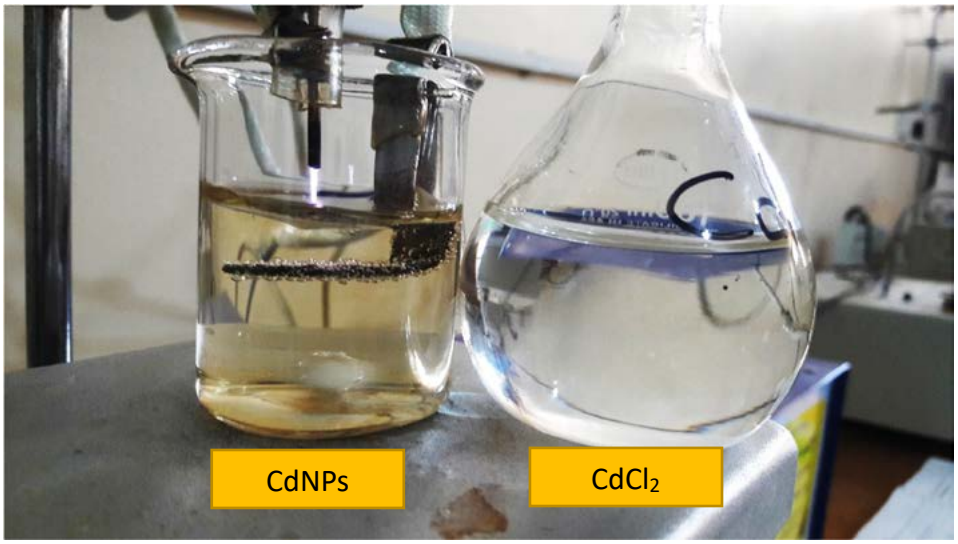

Fig. 3A: symbolizes the formation and color shift of MNPs. Shows how CdNPs.

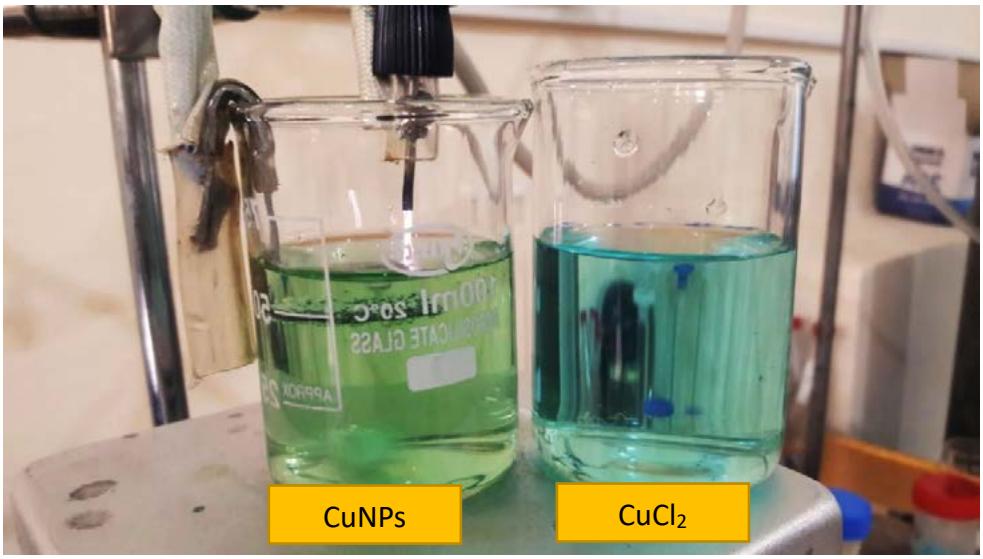

Fig. 3B: symbolizes the formation and color shift of MNPs. Shows how CuNPs.

preparing composites

Following the completion of the graphene oxide preparation process using the Hammer method and the plasma system for nanometals. The following is the procedure used to prepare the nanocomposites: Graphene oxide (GO) is synthesized at a concentration of 1000 ppm with a weight of 1 g of GO in a volumetric flask with a 1000 ml capacity, and deionized water is added. GO/M NPs are mixed in a 10:1 ratio (1000 ppm of GO to 100 ppm of CdNPs and CuNPs). After 10 ml of graphene oxide has been prepared, the volume needed is calculated by making 10 ml with deionized water while taking the desired concentration of 100 ppm and the metal content of the stock into consideration. GO is combined with CdNPs and CuNPs (Composites) in a glass volumetric vial and heated to 25–35 °C for 48 hours while being constantly swirled. The combination (composites) is then subjected to a 15-minute ultrasonic treatment.

GO/MNPs gas sensing method

The nanocomposite samples are thoroughly cleaned using solvents such isopropanol, ethanol,

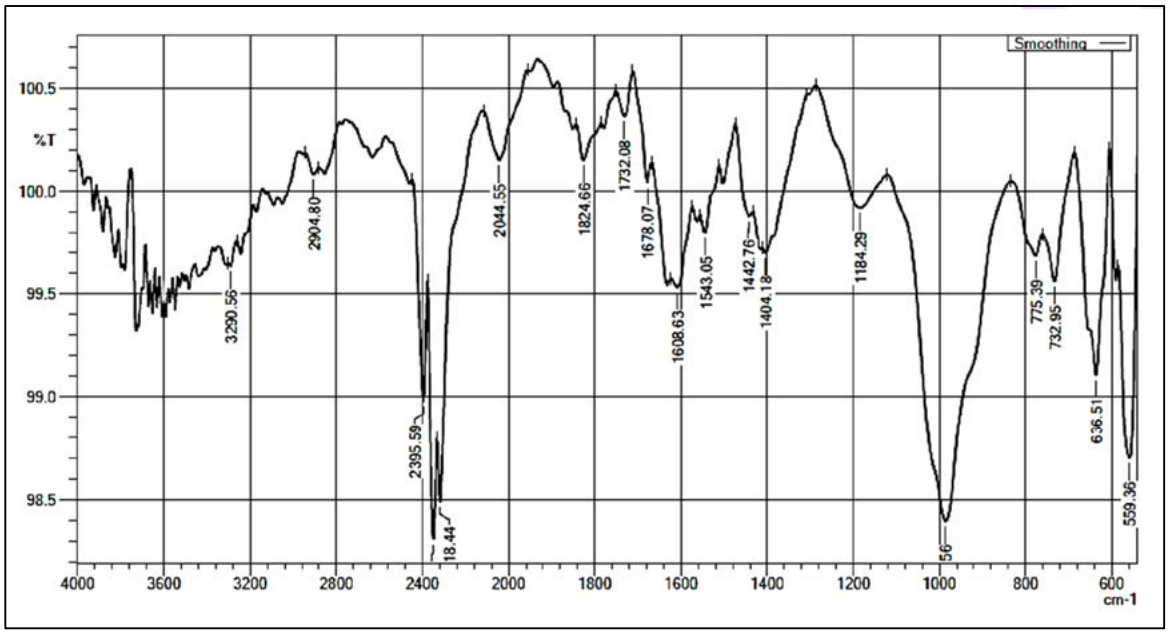

Fig. 4: Shows the graphene oxide FTIR spectrum.

or methanol before being put onto glass or silicon wafers. Films of the nanocomposites having a thickness of 22 nanometers and an area of 50 micrometers are deposited onto the wafers using a dropper. After that, electrodes are installed to secure the sample and move it to an impedance analyzer. After that, each sample is placed inside a sealed system that only allows gases to escape through predetermined openings. This apparatus has an electrical heat source that can be controlled externally and has a temperature range of 0 to 200°C (Revathi et al., 2023). After the gas is fed into the system at a predetermined pressure, the temperature is changed and the resistance is measured at each temperature to carry out the required calculations.

RESULTS AND DISCUSSION

FT-IR analysis of GO

FTIR measurements are crucial for identifying the functional groups in graphene oxide molecules. Graphene oxide and graphite FTIR spectra revealed elastic and bending bands between 600 and 4000 cm^{-1} in wavelength. FT-IR displays the GO spectrum (Fig. 4). The signal at 1586 cm-1 was found to originate from the unoxidized graphitic domain, which is a component of the (C=C) group stretching beam of the aromatic rings, as shown. At 3401.5 cm^{-1}, a broad and powerful band that showed the stretching vibration of the (C-OH, COOH) and H_2O residue appeared. The two bands corresponding to (C-O) stretching were located at 1400.5 cm^{-1} and 1221.94 cm^{-1} (He et al., 2022). Additionally, a beam in the spectrum at 1718 cm^{-1} was discovered to be a component of group C = 0 stretching beam, signifying the synthesis of graphene oxide. A wide, overlapping beam was also observed at 1185 cm^{-1}; this beam is connected to (C-C), (C-O-C) epoxy. The number of COOH groups can be determined using the (O-H) bending vibration of (COOH) groups. Alkoxy (C-OH) groups were subjected to vibration at 1061.13 cm^{-1}. Furthermore, the band at 1724 cm^{-1} may be related to ketones or quinine in addition to the carbonyl group stretching vibration of (COOH) that is positioned at the borders. (He et al., 2022).

UV-visible spectrophotometer for analysis

Research is being conducted on CuNPs and CdNPs. A JASCO V 650 spectrophotometer was used to measure the absorption spectrum of nanoparticles generated in the 200–800 nm wavelength range with a resolution of 1 nm. CuNPs UV-Vis spectra are displayed in Figure 5-A. The large SPR band (surface plasmon resonance) indicated that the nanoparticles were polydispersed.

The formation of NPs was verified by examining the samples' UV-Vis absorption spectra, which revealed spherical CuNPs of 8 nm size where the UV-Vis absorption spectrum displayed a peak at 600 nm and a distinctive surface resonance peak at 478 nm indicates the formation of Cu_2ONPs (Rai et al., 2021). Cadmium oxide nanoparticle production is indicated by the surface

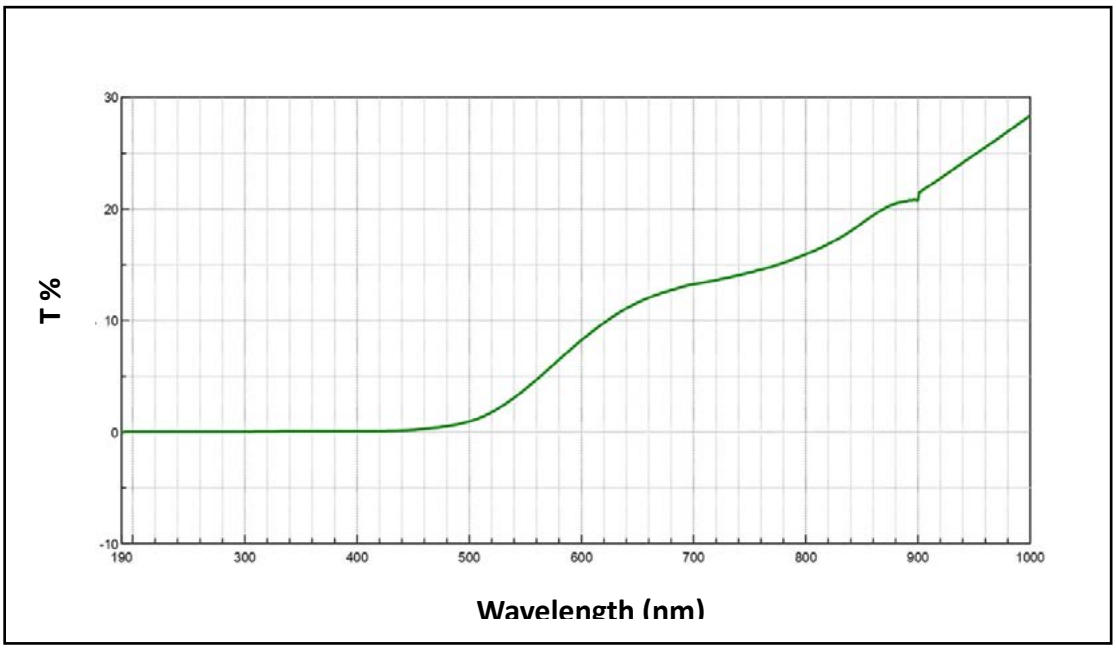

Fig. 5-A: UV-*vis spectrum* of (CuNPs).

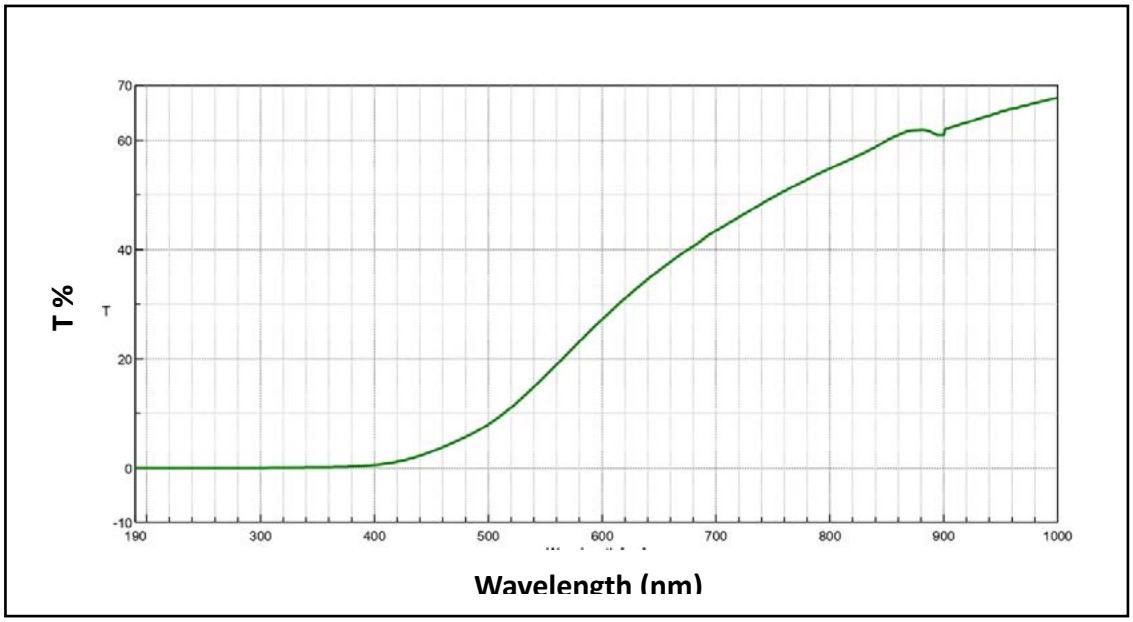

Fig. 5-B: UV-*vis spectrum* of (CdNPs).

resonance peak at 340 nm. The UV absorption spectra shows that cadmium nanoparticles are also indicated by the second peak at 880 nm.

Fig. 5-B. Shows the cadmium nanoparticles' absorption peak in the UV-VIS spectrum. UV-visible spectroscopy is one of the most popular techniques for describing the structure of CdNPs.

Field emission scanning electron microscope (FE-SEM).

FE-SEM measurement is one of the crucial measurements that may be utilized to ascertain nanoscale shapes and diameters. The FE-SEM approach is one way to study the surface morphology of materials. The ray beam emits electrons from an accelerating emission source inside a high vacuum column. The electron beam is then focussed on the sample by passing it via an electromagnetic lens. As a result, several sorts of high-energy electrons are reflected. The peak was created by an elastic collision that took place deep within the sample. An inelastic collision on or near the sample's surface produces secondary electrons, which the detector then gathers to generate an image of the sample's surface. Choosing the right acceleration voltage is essential to creating a high-quality image with a resolution of up to one nanometer. This technique was used to measure graphene oxide's nanodiameters, which were discovered to be between 24 and 35 nm. Alternatively, they have the appearance of stacked nanosheets. Fig. 6 shows graphene oxide FE-SEM images.

FE-SEM pictures of coper nanoparticles large aggregates that resemble quantum dots—made from coper chloride ($CuCl_2$) using a plasma technique are shown in Fig. 7. The enormous clusters of cadmium nanoparticles in Fig. 8. FESEM pictures range in diameter from 19 to 42 nm. They are spherical in shape and group together as though they were a single mass.

Characterization of GO/MNPs

The results demonstrate that GO/CuNPs and GO/CdNPs can offer good surface qualities by adding metallic nanoparticles, such as iron and zinc, into the gaps between GO particles. The composite would benefit from these GO-containing particles' enhanced gas responsiveness and surface resilience to external forces.

XRD Analysis

A PAN analytical (Almedo, Netherlands) X-Pert Pro XRD system was used to analyze GO nanoparticles at 40.0 kV and 30.0 mA. It generates X-rays with a wavelength of 1.54 A° using a graphite monochromator and Cu Ka radiation. The XRD patterns of the G0 are displayed in

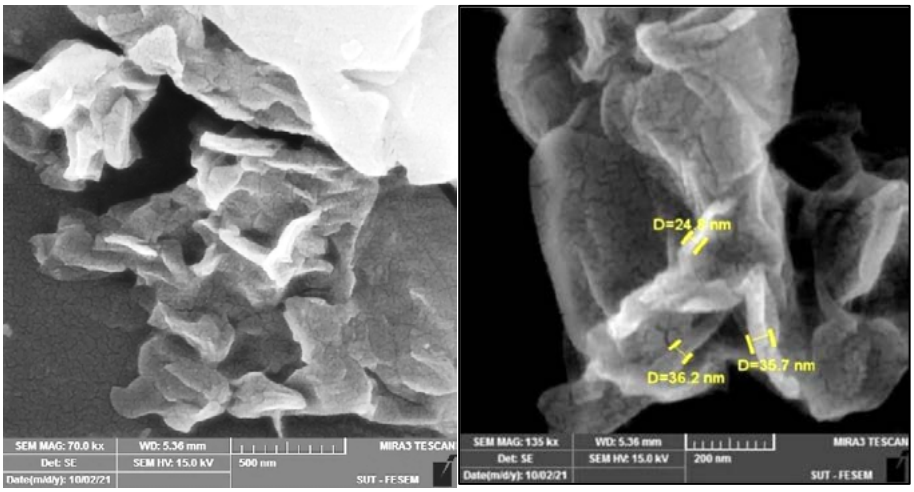

Fig. 6: graphene oxide FE-SEM images are displayed.

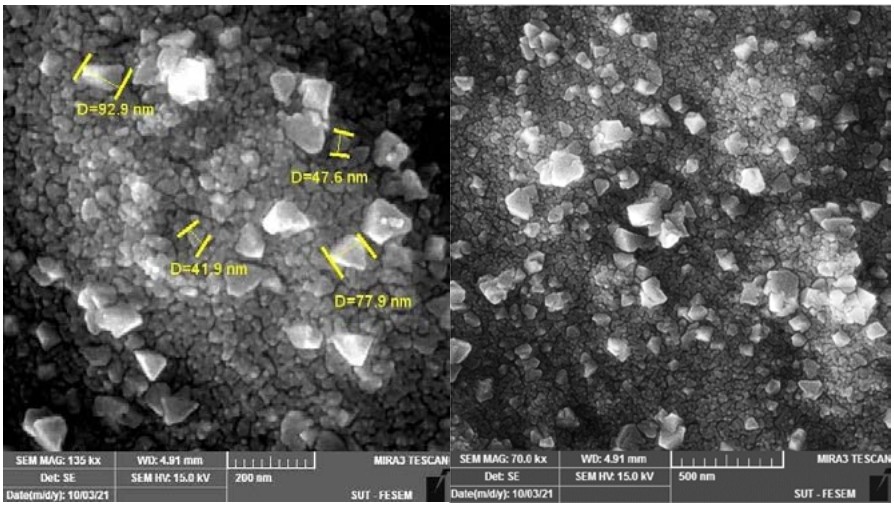

Fig. 7: Represents FE-SEM images of *Coper nanoparticles*.

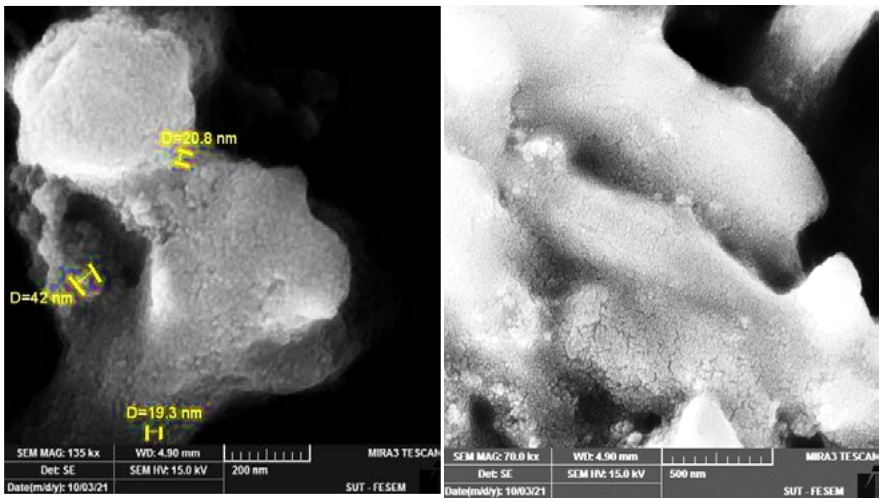

Fig. 8: Represents FE-SEM images of Cadmium *nanoparticles*.

Figure-9 and can be found at 2θ = 11.83, 20.54, 27.06, 35.57, and 42.98. These match the values of Miller's indices: 020, 210, 110, 310, and 420, per ICDD File 9012230 (Hidayah et al., 2017). Fig.-10 displays the XRD patterns of the CuNPs that were produced. XRD analysis was used to confirm the crystalline structure of the CuNPs, revealing the typical Cu peaks at 2θ = 17.3, 34, 31.56, and 57.27. Which, according to (CPDS Card No. 01–078-2076. (Thakar et al., 2022). correspond to the following values of Miller's indices: 111, 221, 212, and 510 .Fig.-11 displays the XRD patterns of the CdNPs that were produced. The typical Cd peaks, which appear at 2θ = 11.56, 14.73, 18.52, 25.24, 26.72, 30.21, 33.26, 36.72, 37.51, 43.67, 46.25 and 58.87, were revealed by XRD analysis, confirming the crystalline structure of the CdNPs. These values correspond to the values of Miller's indices, which are 111, 120, 022, 111, 111, 201, 240, 160, 220, 202, 350 and 315 according to (JCPDS card No. 05-0640) (Mirtamizdoust et al., 2020). Tables (1) show the crystal size values for GO, CuNPs and CdNPs, respectively, calculated using Scherer equation.

EDX Analysis

An essential analysis that goes along with other analyses like XRD, FESEM, and FTIR is

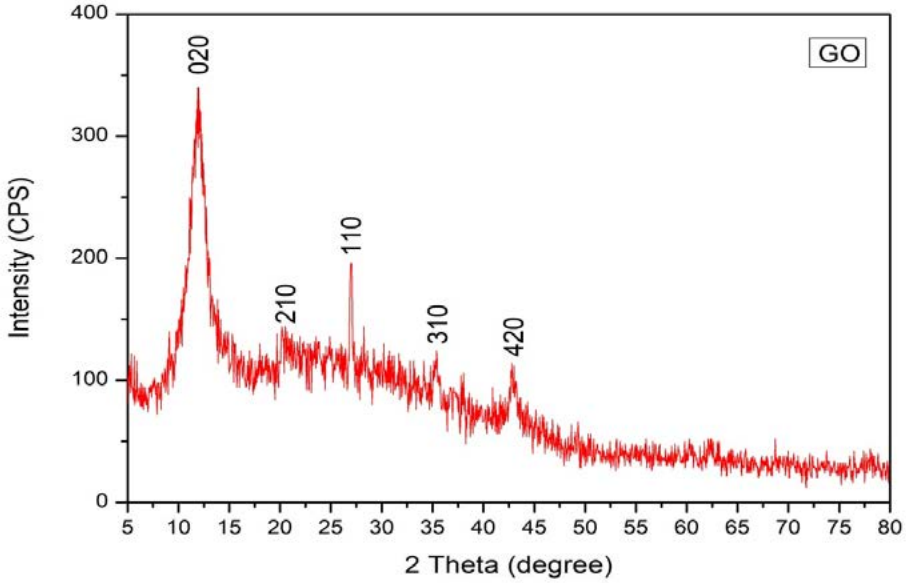

Fig. 9: XRD of *Graphene Oxide*.

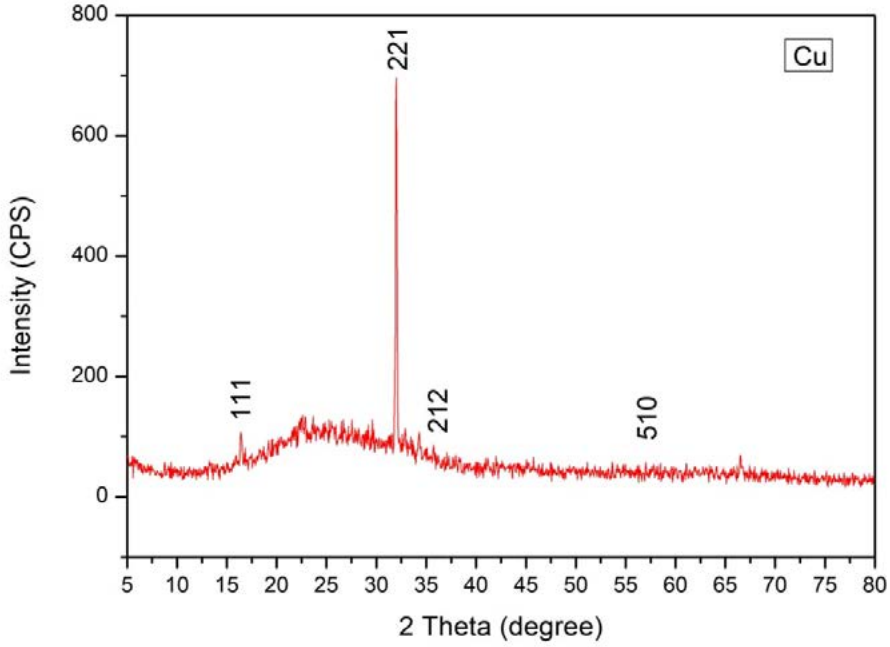

Fig. 10: XRD of A- *CuNPs.*

EDX analysis. The weights and quantities of common and nanoscale elements in any sample can be ascertained via EDX analysis. The weight and percentage of copper nanoparticles in the sample supplied for analysis are displayed in Fig. (12). The weight and percentage of cadmium nanoparticles in the second sample are displayed in Fig. (13).

Application

Gas sensing measurement.

Installing sensors that may detect hazards, like gas sensors, has become essential due to the development of industrial technology. The unique electronic structure of nanomaterials

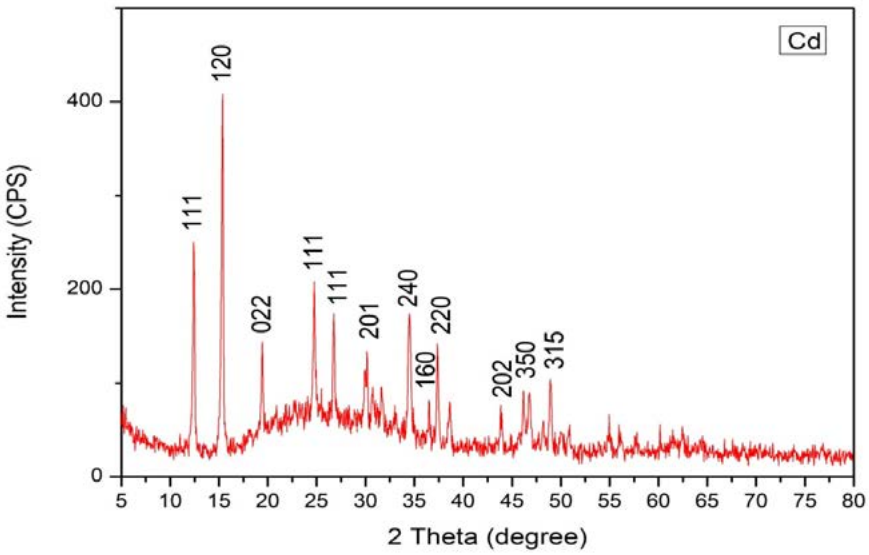

Fig.11: XRD of *CdNPs.*

Table 1: Average and *D.average* of GO, CuNPs and CdNPs

Element	2theta	FWHM	HKI	Average	D.average
GO	11.83	1.7096	020	0.8498236	1.585350
	20.24	1.0330	210	0.9673295	
	27.06	0.8083	110	1.9755050	
	35.57	0.8167	310	2.1405727	
	42.98	0.9750	420	1.9935450	
CuNPs	16.4834	0.2025	111	24.410822	15.495148
	32.0134	0.1636	221	15.557232	
	35.7529	0.1085	212	21.004541	
	53.5399	0.1494	202	3.591256	
	57.0574	0.1150	510	12.91188	
CdNPs	12.4897	0.2086	111	31.274267	38.855886
	15.4095	0.2129	120	24.836480	
	19.4744	0.1800	022	31.273835	
	24.7778	0.2139	111	15.373781	
	26.7864	0.2436	111	91.855488	

determines their conductor, semiconductor, and insulator properties. The vacant d-shells present in transition metal ions enable wide band gaps, superior electrical characteristics, high dielectric constants, and reactive electronic transitions. Consequently, the optoelectronic, optical, electrical, thermal, magnetic, catalytic, mechanical, and photochemical properties of nanocomposites are remarkable and tunable. Additionally, because of their unique shape and size, which exhibit unique physicochemical properties, nanocomposites have a wide range of applications, including sensors, fuel cells, batteries, actuators, supercapacitors, optical devices, pyroelectrics, piezoelectric, ferroelectrics, and random access memory. The concentration of CO gas used is 20 ppm within the operating temperature range (25-200°C). The weight (0.02%) of the sensor material must be proportional to the gas concentration. Conversely, this increase leads to a rapid increase in electrical resistance. Therefore, any increase in the gas concentration while keeping the amount of sensor material constant is pointless because the concentration is sufficient to react with the molecules of the sensor material and to completely cover the surface of the material (Khairnar et al., 2014).

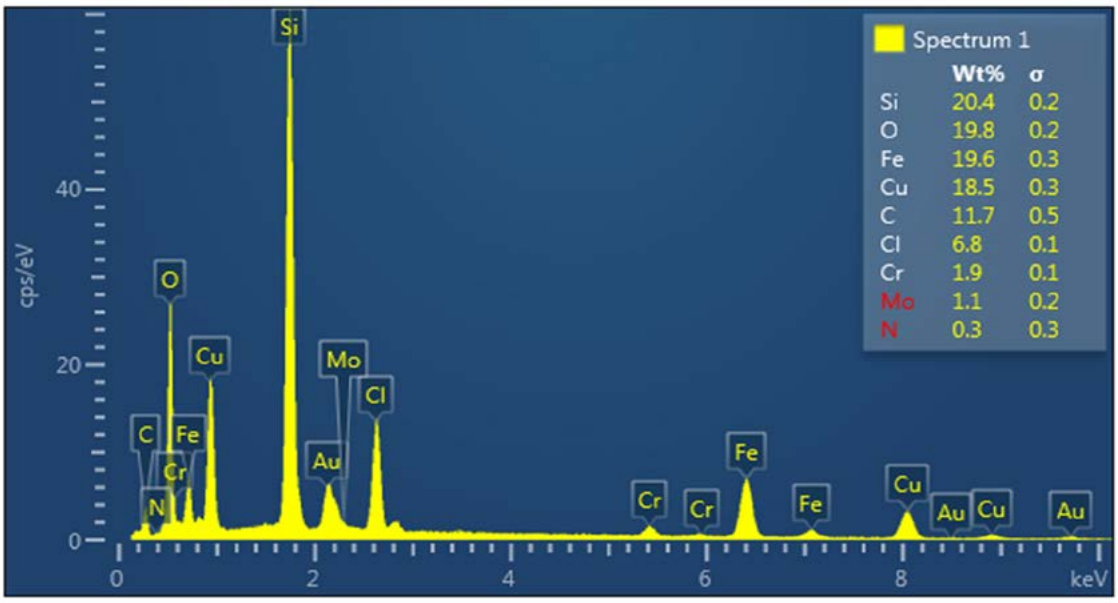

Fig. 12: shows the EDX analysis to determine the percentage and weight *of CuNPs*.

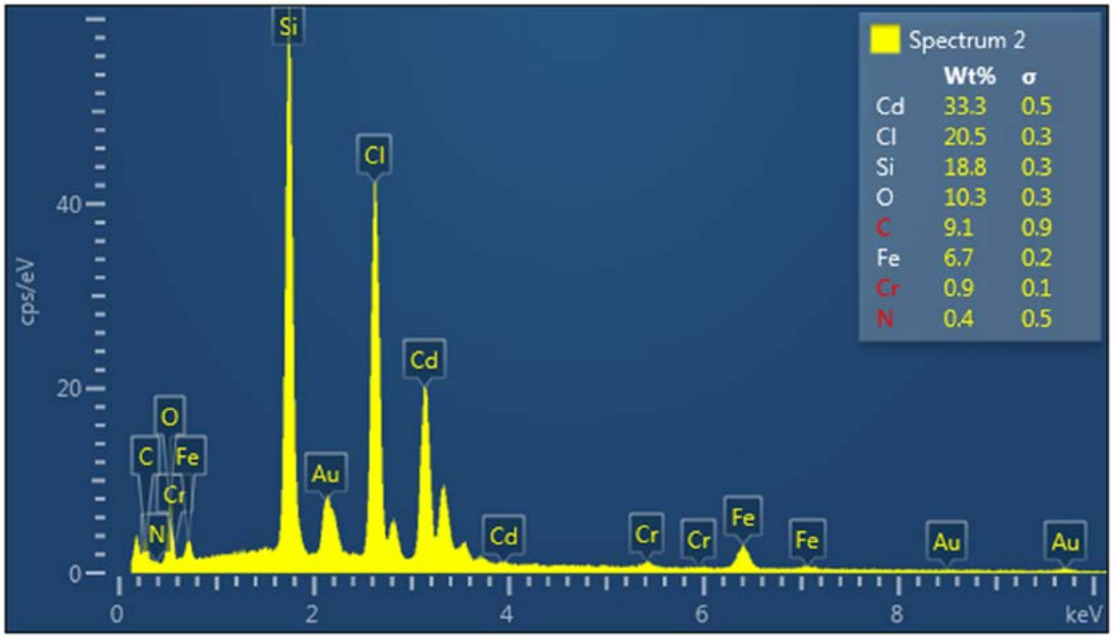

Fig. 13: shows the EDX analysis to determine the percentage and weight *of CdNPs*.

Gas sensitivity of GO/CuNPs and GO/CdNPs and effect of resistance with change in operating temperature by using CO gas

As seen in Fig. 13-A, there is a persistent irregularity in the resistance-time value of the copper nanocomposite GO/CuNPs when measured in seconds at a constant temperature of 200°C. On the other hand, as Fig. 13-B. illustrates resistance values for the cadmium GO/CdNPs nanocomposite decline almost uniformly with time and at the same temperature. This illustrates how temperature clearly affects the stability of nanocomposites.

Sensitivity vs. Time of GO/CuNPs and GO/CuNPs using CO.

Graphene oxide nanocomposites with nanometals in one, two, or three dimensions are

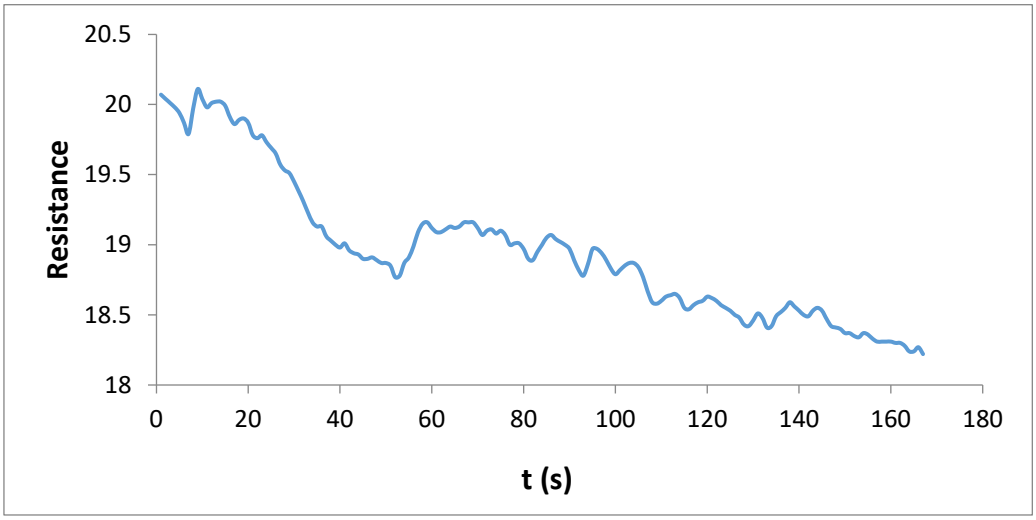

Fig. 13-A: Resistance vs. Time (S) of GO/*CuNPs sensor using CO gas*.

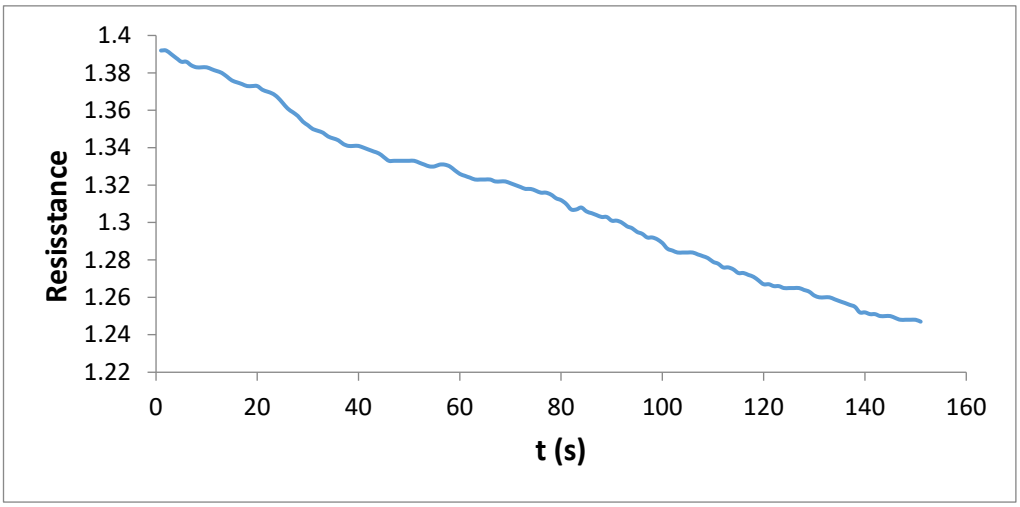

Fig. 13-B: Resistance vs. Time (S) of GO/*CdNPs gas sensor using CO gas*

regarded as effective sensors. Additionally, these nanocomposites have features that set them apart from single-type sensors like graphene oxide or nanometals by themselves. This is because the linkages are mostly found within the nanocomposite's surface area. The interactions between acid groups and gas molecules result in huge aggregations or agglomerations on the surface of the nanocomposite, which give the sensor a high sensitivity value. In addition to the presence of nano-metals and their oxides, graphene oxide provides a vast surface area for detecting the presence of gas by filling all the interstitial gaps between molecules. Temperature clearly affects nanocomposites, and the impact varies depending on the type and nature of the composite. Certain composites work under normal pressure and temperature circumstances, but their chemical instability causes their sensitivity to decrease as the temperature rises. Selective oxidation of volatile organic compounds takes place as a result of the chemical interaction between the gas molecules and the sensor's active groups; the semiconducting substance is of the P-type. Fig. 14-A represents the ratio between operating temperature and sensitivity % values for the GO/CuNPs nanocomposite. The formula used to calculate S% is: **($S\% = R_{on}(\upsilon) - R_{off}(\upsilon) / R_{on}(\upsilon) * S\%$).** The S% at 25°C was 13.564, at 100°C it was 14.882, and at 200°C

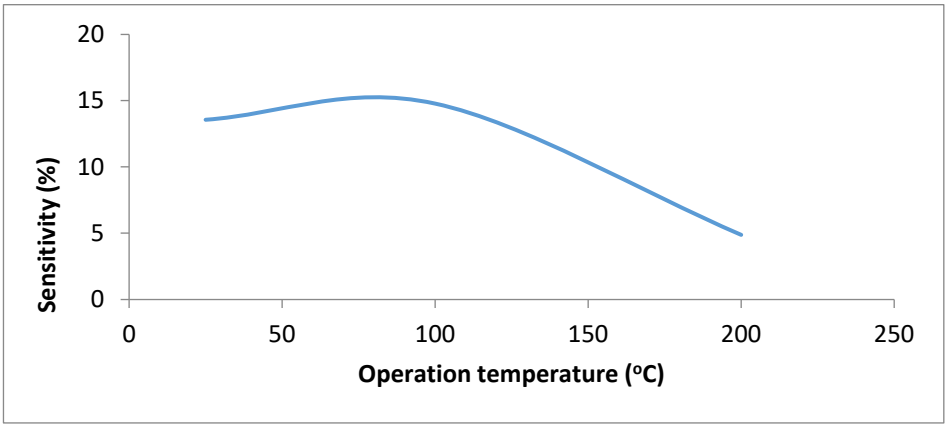

Fig. 14-A: Sensitivity vs. operating temperature of GO/CuNPs *using CO as gas sensing technique.*

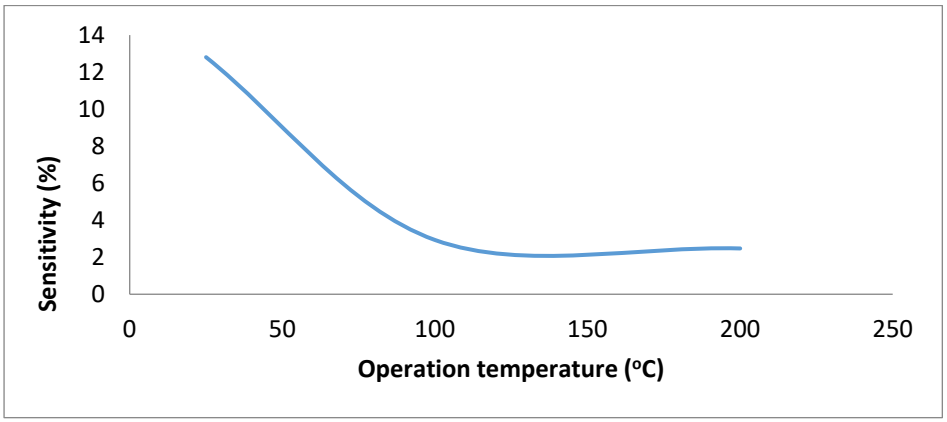

Fig. 14-B: Sensitivity vs. operating temperature of GO/CuNPs *using CO as gas sensing technique.*

Table 2: Represents the values for response time and recovery time versus operating temperature for GO/CuNPs and GO/CdNPs.

Composites	Temp. (°C)	Response time (s)	Recover time (s)
GO/CuNPs	25	24.7	105.3
	100	25.2	90
	200	23.4	39.6
GO/CdNPs	25	31.5	130.5
	100	22.5	67.5
	200	19.8	52.2

it was 4.881. Based on these values. It was observed that as the temperature increased above 25°C, the S% value rose until it reached its highest value at 80°C, where S% was 15.3. After this temperature, S% began to decrease with increasing temperature. This indicates that the copper nanosensor performs best at temperatures below 100°C.

The effect of temperature on response time and recovery time.

When assessing the sensor's quality, response and recovery times are crucial. In terms of responding to any gas leak as quickly as possible. It is important to consider the great selectivity of sensor selection under various settings. Accordingly, the composition, structure, concentration, and type of membrane that each gas operates on are all unique. The response and recovery times are significantly impacted by the gas concentration. It was discovered that the response time is low at high gas concentrations, which provides a good indication of the sensor

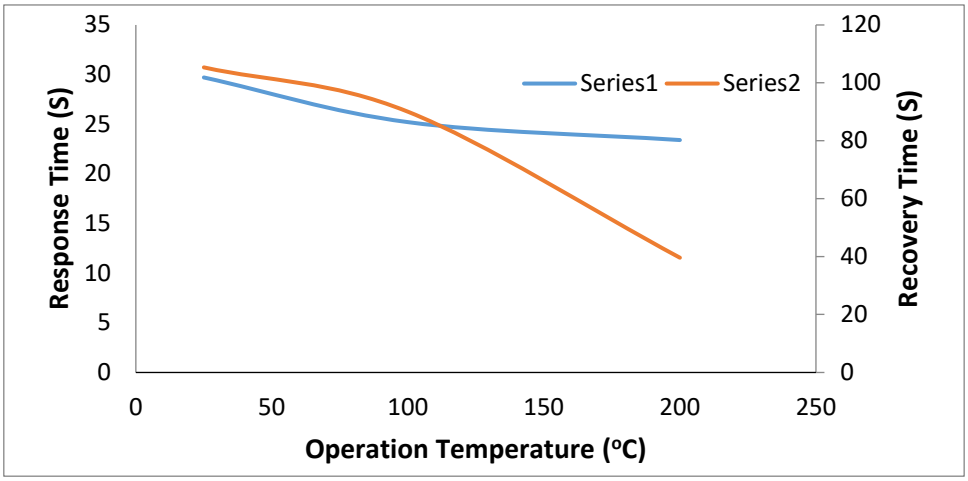

Fig. 15-A: Response time and Recovery time vs. operation temperature of the GO/CuNPs *gas sensor using CO gas*.

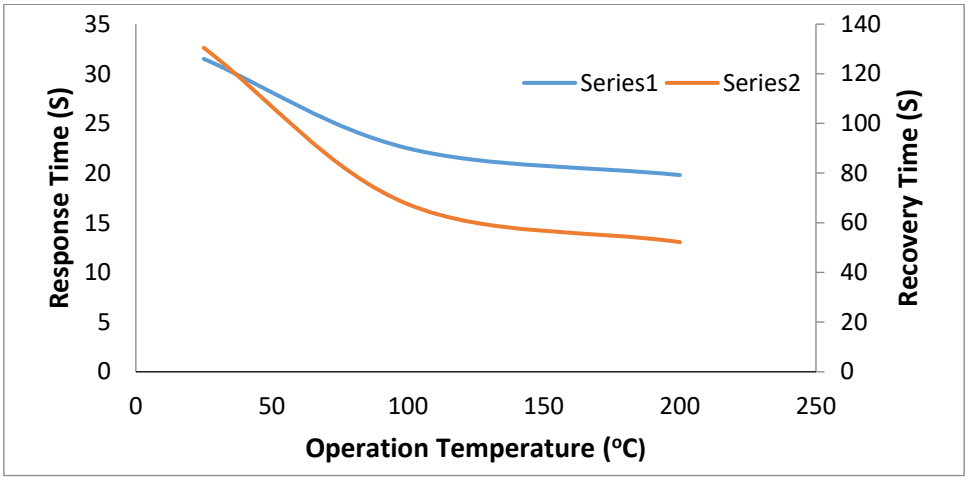

Fig. 15-B: Response time and Recovery time vs. operation temperature of the GO/CdNPs *gas sensor using CO gas*.

that was employed. Additionally, at high concentrations, the recovery time is longer than the reaction time. The structure and content of the gas itself, as well as its impact on the membrane formed from the sensor in terms of thickness and surface area, as well as the membrane's quality and the active groups it contains, cause the response and recovery times to vary from one gas to another. Table (2) represents the values for response time and recovery time versus operating temperature for GO/CuNPs and GO/CdNPs nanocomposites.

By comparing the two nanocomposites, it was found that the copper nanocomposite had an advantage over the cadmium nanocomposite based on the values of response time and recovery time with temperature change. Fig. (15-A) shows the relationship between operating temperature, response time, and recovery time for the GO/CuNPs copper nanocomposite. Fig. (15-B) shows the relationship between response time, recovery time, and operating temperature for the GO/CdNPs cadmium nanocomposite.

CONCLUSION

Carbon monoxide is a toxic oxide, so solutions must be found to address leaks at their sources. One such solution is the development of nanocomposites for gas sensing. Measurements have shown that the concentration is related to the amount of the substance, meaning the gas

concentration must completely coat the substance molecules through interaction. The CO gas was tested on copper and cadmium nanocomposites prepared from graphene oxide with specific concentrations of nanometals. A comparison between the copper nanocomposite (GO/CuNPs) and the cadmium nanocomposite (GO/CdNPs) revealed that the copper nanocomposite was superior. Based on the resistance, sensitivity (%), response time, and recovery time values we obtained, this application was conducted at temperatures ranging from 25°C to 200°C. It is noted through the practical results that there is a discrepancy in the values of resistance (increase or decrease in its value) compared to temperatures. These composites have the potential to be at the forefront of materials utilized for sensitivity and gas detection under various temperature settings. It is possible to prevent the threat posed by the propagation of these gasses at the early stages of their occurrence. The values of response time and recovery time versus operation temperatures showed that these composites have a specificity in response. Along with the vast range of these values in relation to operating temperatures, there are also relative sensitivity values. They are therefore popular sensors in the field of gas detection.

ACKNOWLEDGMENTS

We would like to express our gratitude to Anbar University's College of Science and Department of Chemistry for providing their researchers with the equipment and facilities they need, as well as for continuously monitoring the completion of scientific study. In addition to thanks and appreciation to the Pollution Journal, which focuses on research papers related to addressing environmental pollution.

CONFLICT OF INTEREST

The author declares no conflict of interest. This work can enhance the reduction of the spread of toxic substances before they reach unacceptable concentrations by placing sensors in areas where the gas is present to predict the danger.

LIFE SCIENCE REPORTING

Research papers similar to this work can promote the establishment of basic steps for entering the field of environmental life sciences and provide appropriate solutions for that.

REFERENCES

Altammar, K. A. (2023). A review on nanoparticles: characteristics, synthesis, applications, and challenges. *Frontiers in microbiology*, *14*, 1155622.

Chen, F., Yan, T. H., Bashir, S., & Liu, J. L. (2022). Synthesis of nanomaterials using top-down methods. *Advanced nanomaterials and their applications in renewable energy*, 37-60.

Chen, S., Fan, S., Qiao, Z., Wu, Z., Lin, B., Li, Z., ... & Lim, C. T. (2025). Transforming healthcare: Intelligent wearable sensors empowered by smart materials and artificial intelligence. *Advanced Materials*, 2500412.

Coiai, S., Campanella, B., Paulert, R., Cicogna, F., Bramanti, E., Lazzeri, A., ... & Coltelli, M. B. (2021). Rosmarinic acid and Ulvan from terrestrial and marine sources in anti-microbial bionanosystems and biomaterials. *Applied Sciences*, *11*(19), 9249.

Ding, Y., Wang, C., Zeng, M., & Fu, L. (2025). Atomic manufacturing of advanced nanomaterials. *Advanced Materials*, *37*(31), 2306689.

Dulta, K., Virk, A. K., Chauhan, P., Bohara, P., & Chauhan, P. K. (2022). Nanotechnology and applications. In *Applications of computational intelligence in multi-disciplinary research* (pp. 129-141). Academic Press.

El-Naggar, M. E., Ullah, S., Wageh, S., Abu-Saied, M. A., Khattab, T. A., Alhashmialameer, D., ... & Matter, E. A. (2023). Preparation of epoxy resin/rare earth doped aluminate nanocomposite toward photoluminescent and superhydrophobic transparent woods. *Journal of Rare Earths*, *41*(3), 397-405.

Fanelli, F., & Fracassi, F. (2014). Aerosol-assisted atmospheric pressure cold plasma deposition of organic–inorganic nanocomposite coatings. *Plasma Chemistry and Plasma Processing*, *34*(3), 473-487.

Gao, Z., Wei, J., Hu, X., Yang, X., Ling, K., Li, G., ... & Xia, Y. (2025). Review of Narrow-Bandgap Infrared Quantum Dots Solar Cells. *Solar RRL*, e202500640.

Gao, Z., Yang, S., Ma, Y., Wei, T. R., Chen, X., Zheng, W., ... & Shi, X. (2025). Warm metalworking for plastic manufacturing in brittle semiconductors. *Nature Materials*, 1-7.

Geng,L., & Luo, Z. (2024). Magnetic metal clusters and superatoms. *The Journal of Physical Chemistry Letters*, *15*(7), 1856-1865.

He, Q., Liu, J., Zhang, M., Zhai, Z., & Jiang, B. (2022). Molecular Dynamics Simulation on the effect of self-resistance electric heating on carbon fiber surface chemical properties and fiber/PP interfacial behavior. *Polymers*, *14*(5), 1043.

Hidayah, N. M. S., Liu, W. W., Lai, C. W., Noriman, N. Z., Khe, C. S., Hashim, U., & Lee, H. C. (2017, October). Comparison on graphite, graphene oxide and reduced graphene oxide: Synthesis and characterization. In *AIP Conference Proceedings* (Vol. 1892, No. 1, p. 150002). AIP Publishing LLC.

Khairnar, R. S., Anjum, S. R., Kokol, V., & Mahabole, M. P. (2014). Carbon nanotube doped nano-hydroxyapatite sensor matrix for gas sensing application. *International Journal of Modern Communication Technologies & Research*, *2*(4), 29-34.

Khan, W. S., Asmatulu, E., & Asmatulu, R. (2025). Nanotechnology emerging trends, markets and concerns. In *Nanotechnology safety* (pp. 1-21). Elsevier.

Koohkansaadi, G., Tabean, M., Mohagheghi, A., Masoumi, S., Jahanabad, Z. J., Mobed, A., & Charsouei, S. (2025). Aspirin nanosensors. *Clinica Chimica Acta*, 120222.

Kumar, R., Rakesh, A. K., Yogi, R., Govindan, A., & Jaiswal, N. K. (2022). First-principles study of CO adsorption on zigzag ZnO nanoribbons towards nanosensor application. *Journal of Molecular Graphics and Modelling*, *116*, 108232.

Lines, M. G. (2008). Nanomaterials for practical functional uses. *Journal of Alloys and Compounds*, *449*(1-2), 242-245.

Liu, X., Chen, S., Zhang, Y., Liu, M., Emori, W., & Shao, Y. (2021). Preparation of graphene oxide–boron nitride hybrid to reinforce the corrosion protection coating. *Corrosion Reviews*, *39*(2), 123-136.

López-Hernández, F. J. (2021). Cell surface area to volume relationship during apoptosis and apoptotic body formation. *Cell. Physiol. Biochem*, *55*, 161-170.

Lowry, P. B., Boh, W. F., Petter, S., Leimeister, J. M., & Guest Editors. (2025). Long Live the Metaverse: Identifying the potential for market disruption and future research. *Journal of Management Information Systems*, *42*(1), 3-38.

Malik, S., Muhammad, K., & Waheed, Y. . (2023). Nanotechnology: a revolution in modern industry. *Molecules*, *28*(2), 661

Mirkin, C. A., Petrosko, S. H., Artzi, N., Aydin, K., Biaggne, A., Brinker, C. J., ... & Zhu, W. (2025). 33 Unresolved Questions in Nanoscience and Nanotechnology.

Mirtamizdoust, B., Hanifehpour, Y., Behzadfar, E., Sadeghi-Roodsari, M., Jung, J. H., & Joo, S. W. (2020). A novel nano-structured three-dimensional supramolecular metal-organic framework for cadmium (II): A new precursor for producing nano cadmium oxide. *Journal of Molecular Structure*, *1201*, 127191.

Naseem, Z., Ayub, A. R., Arshed, S. M., Afzal, F., Arif, S., Raza, U., ... & Hamid, H. (2025). Carbon Nanocone Oxide-mediated controlled interaction to increase Favipiravir's bioavailability: an extensive in silico research. *Computational Biology and Chemistry*, 108756.

Oehrlein, G. S., Brandstadter, S. M., Bruce, R. L., Chang, J. P., DeMott, J. C., Donnelly, V. M., ... & Ventzek, P. L. (2024). Future of plasma etching for microelectronics: Challenges and opportunities. *Journal of Vacuum Science & Technology B*, *42*(4).

Omanović-Mikličanin, E., Badnjević, A., Kazlagić, A., & Hajlovac, M. (2020). Nanocomposites: a brief review. *Health and Technology*, *10*(1), 51-59.

Orangi, S., Manjong, N., Clos, D. P., Usai, L., Burheim, O. S., & Strømman, A. H. (2024).Historical and prospective lithium-ion battery cost trajectories from a bottom-up production modeling perspective.

Journal of Energy Storage, *76*, 109800.

Pan, L., Guo, Z., Li, H., Wang, Y., Rao, H., Jian, Q., ... & Wei, L. (2024). High-Performance Porous Electrodes for Flow Batteries: Improvements of Specific Surface 6-Areas and Reaction Kinetics. *ChemElectroChem*, *11*(21), e202400460.

Rai, R., & Chand, D. K. (2021). Copper nanoparticles (CuNPs) catalyzed chemoselective reduction of nitroarenes in aqueous medium. *Journal of Chemical Sciences*, *133*(3), 87.

Rashid, A.(2024). Review of:" Normally, the length of nanowires is more than 1000 times greater than their diameter. This huge difference in ratio (length to diameter) *compared to nanowires is often referred to as D materials"*.

Rashid, H. A., & Hassan, N. E. (2024). Review of toxic gases and their impact on human health. *Jabirian Journal of Biointerface Research in Pharmaceutics and Applied Chemistry*, *1*(4), 7-12.

Revathi, B., Perumal, P., & Deivamani, D. (2023). Optical and Gas Sensing Properties of Pr-Doped TiO_2 Thin Film. *Iranian Journal of Materials Science and Engineering*, *20*(2).

Ruiz, V. H., Encinas-Basurto, D., Ortega-Alarcon, N., Eedara, B. B., Fineman, J. R., Black, S. M., & Mansour, H. M. (2024). Inhalable advanced Co-spray dried microparticles/nanoparticles of a novel RhoA/rho kinase inhibitor with lung surfactant biomimetic phospholipids for targeted lung delivery. *ACS Pharmacology & Translational Science*, *7*(10), 3241-3254.

Salim, E., Abdelghany, A. M., & Tarabiah, A. E. (2024). Ameliorating and tuning the optical, dielectric, and electrical properties of hybrid conducting polymers/metal oxide nanocomposite for optoelectronic applications. *Materials Chemistry and Physics*, *313*, 128788.

Thakar, M. A., Jha, S. S., Phasinam, K., Manne, R., Qureshi, Y., & Babu, V. H. (2022). X ray diffraction (XRD) analysis and evaluation of antioxidant activity of copper oxide nanoparticles synthesized from leaf extract of Cissus vitiginea. *Materials Today: Proceedings*, *51*, 319-324.

Tofail, S. A., Koumoulos, E. P., Bandyopadhyay, A., Bose, S., O'Donoghue, L., & Charitidis, C. (2018). Additive manufacturing: scientific and technological challenges, market uptake and opportunities. *Materials today*, *21*(1), 22-37.

Upadhyay, G., Saxena, K. K., Sehgal, S., Mohammed, K. A., Prakash, C., Dixit, S., & Buddhi, D. (2022). Development of carbon nanotube (CNT)-reinforced Mg alloys: fabrication routes and mechanical properties. *Metals*, *12*(8), 1392.

Vargas, S. A., Delgado-Macuil, R. J., Ruiz-Espinosa, H. É. C. T. O. R., Rojas-López, M. A. R. L. O. N., & Amador-Espejo, G. G. (2021). High-intensity ultrasound pretreatment influence on whey protein isolate and its use on complex coacervation with kappa carrageenan: Evaluation of selected functional properties. *Ultrasonics Sonochemistry*, *70*, 105340.